

# APPLICATION OF ADVANCED SURFACE SENSORS FOR THE DETECTION AND CONTROL OF FLOW SEPARATION ON AN INDUSTRIAL HIGH-LIFT CONFIGURATION

L. Hoefener<sup>1</sup>, J. Leuckert<sup>1</sup>, K.-P. Neitzke<sup>2</sup>, M.J. Hucker<sup>3</sup>, C. Warsop<sup>3</sup>, W. Nitsche<sup>1</sup>

<sup>1</sup> Institute of Aeronautics and Astronautics, Berlin University of Technology, Germany,

<sup>2</sup> AIRBUS Deutschland GmbH, Bremen, Germany,

<sup>3</sup> BAE SYSTEMS Advanced Technology Centre - Sowerby, Filton, Bristol, UK,

**Keywords:** MEMS, advanced surface sensors, flow separation and transition detection, high-lift flow control

## Abstract

This paper describes the results of experimental investigations on the characterisation of transition and flow separation on a slat of an industrial high-lift configuration by means of advanced flush-mounted surface sensors. Passive vortex generators and active devices were applied on the leading edge in order to control the flow separation. The wind tunnel tests were performed in the DNW-NWB low-speed wind tunnel in Braunschweig using a three-element 2D model in a take-off configuration at Mach numbers  $M_\infty = 0.1$  ( $Re = 1.5 \cdot 10^6$ ) and  $M_\infty = 0.2$  ( $Re = 3 \cdot 10^6$ ). The results presented characterise the flow conditions using surface arrays of hot-wire sensors as well as miniaturised MEMS sensors developed during the European Project Aeromems II. For the base flow, the sensor signals indicate a range of boundary layer transition at low angles of attack  $\alpha$ , whereas at higher  $\alpha$  flow separation takes place. The application of flow control devices delays the turbulent separation and improves the post-stall behaviour.

## 1 Nomenclature

$\alpha$	angle of attack
$\eta$	deflection angle
$c_l$	lift coefficient
$\hat{c}_{p_{max}}$	normalized pressure coefficient
$M$	Mach number
$max$	maximum
$p_{chamber}$	pressure measured in actuator chamber
$Re$	chord Reynolds number
$St_{c_{slat}}$	Strouhal number (slat chord)

## 2 General Introduction

The aerodynamic design of state-of-the-art transport aircraft requires a thorough optimisation of the high-lift configuration in order to realise the necessary take-off and landing lift. The resulting geometry with large angles of attack causes a flow with an adverse pressure gradient at the risk of flow separation. On a slat in particular, even a laminar separation bubble may occur [1]. The usage of dedicated high-lift devices, such as a slat or a flap, increases the maximum lift but also the drag, the weight and the system complexity. Vortex generators, turbulators and passive transpiration are widely used today to suppress a laminar separation bubble and delay flow separation. A new approach to gain the benefits of an effective high-lift system without a massive weight and maintenance penalty is the applica-

tion of flow control devices [7, 6]. This allows the simplification of the high-lift devices and the reduction of the airframe-noise during approach. Moreover, this potentially makes it possible to design heavier and more stretched variations of existing aircraft using the same high-lift system.

In order to control the separated flow, the leading edge of the investigated high-lift configuration was equipped with both passive vortex generators and active devices to avoid flow separation by forcing the laminar-turbulent transition to intensify the turbulent mixing. Robust and sensitive sensors are required to monitor the flow for in-flight applications and to identify the relevant large coherent structures [9]. Therefore, the present investigations mainly focused on the characterisation of flow regimes on an industrial high-lift configuration using advanced surface sensors. The application of signal analysis methods allowed the detection of laminar-turbulent transition and separation on the leading edge slat. A 2D model was fitted with surface-mounted hot-wires and new miniaturised MEMS flow sensors developed during the Aeromems II project. The MEMS devices were validated by comparing simultaneous measurements carried out using hot-wire sensors and pressure taps. The angle of attack was varied between  $-4^\circ \leq \alpha \leq +21^\circ$ . From results of former experimental investigations on the characterisation of the base flow it is known that a laminar separation bubble occurred at moderate angles of attack, while a turbulent trailing edge separation emerged after reaching the maximum lift [3].

### 3 Set-up

The measurements were carried out in the DNW-NWB low-speed wind tunnel in Braunschweig on a slat of the H8Y high-lift configuration (Airbus Germany, Fig. 1). The 2D model consists of a slat, a main wing and a flap, and has a wingspan of 2.8 m and a chord length of  $c = 0.75$  m in high-lift configuration (clean chord length of 0.6 m). All tests were carried out at Mach numbers  $M_\infty = 0.1$  ( $u_\infty = 34$  m/s) and  $M_\infty = 0.2$  ( $u_\infty = 68$  m/s),  $Re = 1.5 \cdot 10^6$  and

$Re = 3 \cdot 10^6$  respectively, in take-off configuration ( $\eta_{Slat} = 20^\circ, \eta_{Flap} = 25.36^\circ$ ). For each Mach number the angle of attack of the main wing was varied between  $-4^\circ \leq \alpha \leq +21^\circ$  ( $\Delta\alpha = 1^\circ$ ).

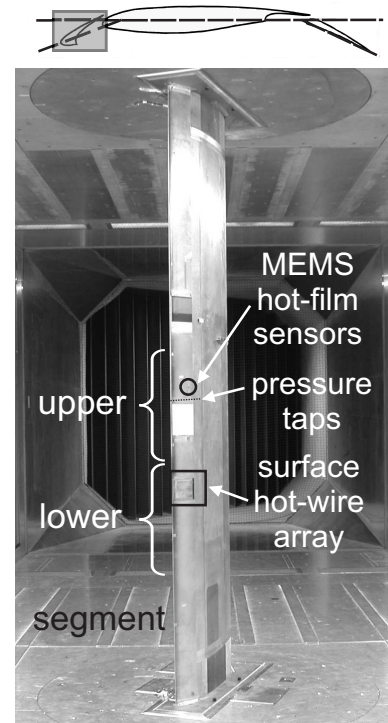


Fig. 1 Set-up of wind-tunnel test at NWB

The suction side was equipped with a span-wise MEMS hot-film sensor array at  $x/c_{Slat} = 0.78$  and a stream-wise array of 32 surface hot-wire sensors ( $0.24 \leq x/c_{Slat} \leq 0.88$ ) to monitor the flow conditions. The sensor signals were recorded and reduced using a high-speed 14-bit multi-channel data-acquisition system, which allows a simultaneous conversion of static and dynamic signals.

Two different nose-inserts were deployed during the wind-tunnel test, one for passive vortex generators and one for an active blowing device consisting of a small air chamber and drilled holes. Since each insert had a distinctive position it was fabricated for, the equipped slat cuts into two areas. The MEMS-sensors as well as the pressure taps were placed downstream of the upper nose-inserts segment, whereas the surface

hot-wire array was applied downstream of the lower segment (Fig. 1).

### 3.1 Flow sensors

In order to minimise sensor-induced surface roughness and curvature modifications, the sensor arrays were flush-mounted into a cavity machined into the upper surface of the slat.

**MEMS hot-film sensors:** Prototype MEMS hot-film sensors were developed and manufactured by BAE Systems Advanced Technology Centre. The sensors consisted of 280 nm thick tungsten film sensing elements of 1 mm length (or 500  $\mu\text{m}$  length; not used during the test campaign) and a 10:1 aspect ratio with a nominal resistance of 6–7  $\Omega$ . These sensing elements were fabricated on a silicon oxide/polyimide/silicon oxide membrane, which provides mechanical support and thermal insulation from the silicon substrate. Electrical connections to the sensor were made by a novel through-wafer via technique, which allowed electrical connections to be placed at the rear of the device resulting in a clean, flat-top surface, to minimise disturbance to the flow examined. Advanced fabri-

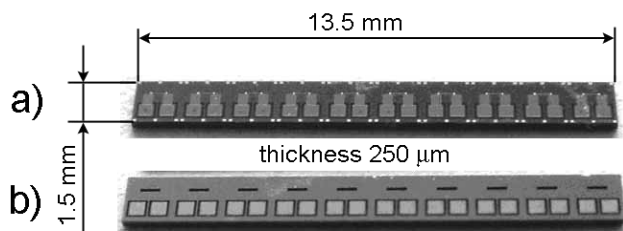


**Fig. 2** Ten individual sensors are incorporated on each chip. Views of MEMS sensor 'chip': a) Front view: sensor 1 to 10 (from the left to the right), b) Rear view

cation techniques were developed to allow the parasitic resistance of the electrical connections to be reduced to less than 0.5  $\Omega$ . Ten devices were placed on each device 'chip' permitting both multiple measurements and redundancy in the event of failure. These devices were placed

on 1.35 mm centres with chip dimensions of 13.5 mm x 1.5 mm x 250  $\mu\text{m}$ . When packaged,

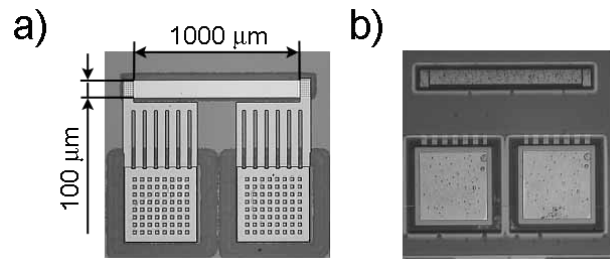


**Fig. 3** Close up of single hot-film sensor: a) Top surface, sense element, b) Lower surface showing rear side electrical connections and sense element through transparent membrane.

the chips fitted into a cut-out section of the test piece so that it was possible to achieve a continuous surface with no steps or gaps. The devices had a measured frequency response in the range 20-30 kHz depending on the configuration of the sense element. The efficiency of the devices was a priority during the design phase, as multiple sensors might be required for an integrated flow control system. Thermal management features incorporated into the design of the sensor increased the amount of energy convected to the airflow from around 1% of the total input for early device iterations to around 20-30% of the total input for the final iteration used in the tests discussed here. At an overheat ratio of 1.3, power consumption for each device was approximately 85 mW at 0 m/s. At an overheat ratio of 1.5, power consumption at 0 m/s was approximately 145 mW rising to around 340 mW at 240 m/s.

The MEMS hot-film sensor array was applied at the chord-wise position  $x/c_{slat} = 0.78$ . The electrical connections to the sensors were laid along the lower surface of the slat and were connected to micro-coax-cables. The sensors were operated in constant temperature mode using a multi-channel anemometer (M-CTA).

**Surface hot-wire sensors:** The surface hot-wire sensors consist of a platinum-coated tung-

sten wire ( $d = 5 \mu\text{m}$ ) welded over a narrow cavity ( $w \approx 80 \mu\text{m}$ ) in order to reduce the heat flux into the wall [8].

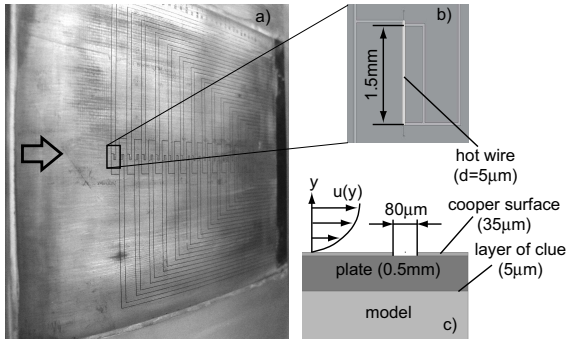


**Fig. 4** Array of 32 surface hot-wire sensors

The sensor array was applied into a cavity machined into the surface of the slat. A vacuum-gluing method assured the flush-mounting of the array consisting of 32 chord-wise sensors (stream-wise spacing  $s = 2.5 \text{ mm}$ , coverage  $0.24 \leq x/c_{Slat} \leq 0.88$ ). Micro-coax-cables were laid along the shroud of the slat close to the trailing edge for connection to the M-CTA to minimize the influence on the flow field.

**Signal analysis:** In order to characterise the different flow properties, the dynamic signals measured were analysed using different statistical quantities. For the non-calibrated sensors used, the DC-values represent relative levels of the quasi wall-shear stress. During the laminar-turbulent transition, the wall-shear stress levels increase significantly [2]. Within the separation region, the wall-shear stress drops and reaches negative values (backflow) [5], but the hot-wire sensor signals are always non-directional absolute values. Zones of increased fluctuation can be identified by analysing the AC-values. Increased AC-values indicate regions of high local fluctuations, such as the laminar-turbulent transition range or the recirculation zone which are characterised by highly oscillating flow conditions [4]. The RMS (Root Mean Square) value was calculated in order to obtain information on the mean fluctuation amplitude in certain areas

of the slat. Increased RMS-values indicate regions with high levels of local fluctuations, e.g. a transition area. Furthermore, a region of separated flow with highly oscillating flow and increased intermittency values is characterised by a high RMS-level [1].

### 3.2 Flow control devices

In order to attenuate the flow separation both *passive vortex generators (VG's)* [5] and *active devices* [6] were deployed at the leading edge of the slat in front of the sensor arrays. Both of them cause longitudinal vortices and increase the momentum transfer. There were two different nose-inserts, one with changeable passive vortex generators and another one containing an active air distributor (Fig. 5).

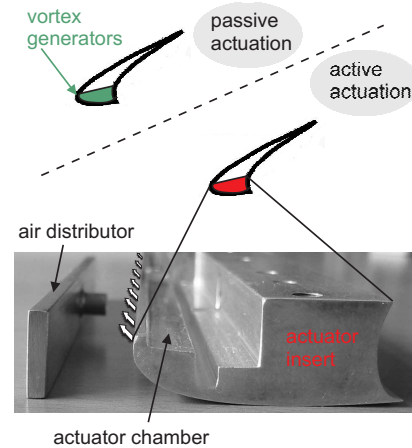


**Fig. 5** Scheme of the nose-inserts

Whilst passive vortex generators are known to be effective in controlling separation and are simple to apply, they often incur a penalty in terms of increased drag when not in use, a factor that is especially relevant for commercial reasons, when the aircraft is cruising. Active flow control devices, on the other hand, do not incur such a drag penalty as they can be de-activated during this part of the flight envelope. Consequently, in addition to vortex generators, tests were carried out to study the effect of pulsed actuation. The former were a Kapton foil device (VG1, height of  $h = 0.08 \text{ mm}$ , Fig. 6a), deliv-

ered by the EADS - Corporate Research Centre (CRC Munich). Furthermore, a self-adhesive aluminium tape with an embossed line of pyramids (VG2, height of  $h = 0.3$  mm, Fig. 6b) was tested.

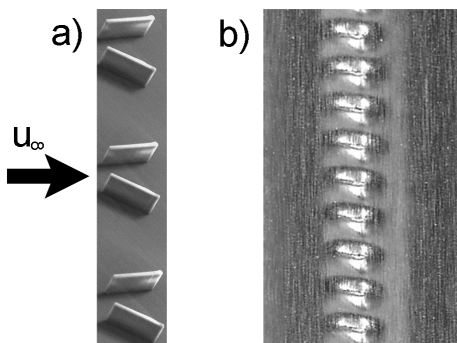


Fig. 6 Passive vortex generators: a) VG1, b) VG2

For the latter, a fast magnetic valve, which was connected to a pressurised air supply and mounted on a slat track, generated a pulsed air flow at the leading edge of the slat. The air distributor in the nose insert linked the pressure chamber with the drilled holes ( $d = 0.5$  mm, spacing  $t = 5$  mm), resulting in an air jet.

## 4 Results

A characterisation of the base flow was performed in order to validate the new MEMS-sensors and to study the influence of the different passive and active flow control devices on the slat flow. Therefore the vortex generators were removed from the nose-insert for passive actuation providing a clean nose and it was changed between the upper and the lower segment.

### 4.1 Base flow

The RMS values of all span-wise staggered MEMS-sensors obtained at  $M_\infty = 0.2$  without flow control devices are shown in Fig. 7. The low RMS-levels for low angles of attack ( $\alpha \leq 4^\circ$ ) clearly indicate an attached laminar flow at the sensor position of the suction side. The transition apparently occurs downstream of the sensor position. Increasing the angle of attack up to

$\alpha = 5^\circ$  results in an upstream shift of the laminar-turbulent boundary layer transition, which passes the sensor position. The rapid growth of the RMS values between  $4^\circ < \alpha < 5^\circ$  and their nearly constant levels up to  $\alpha \leq 10^\circ$  characterise the fully turbulent flow at the sensor position.

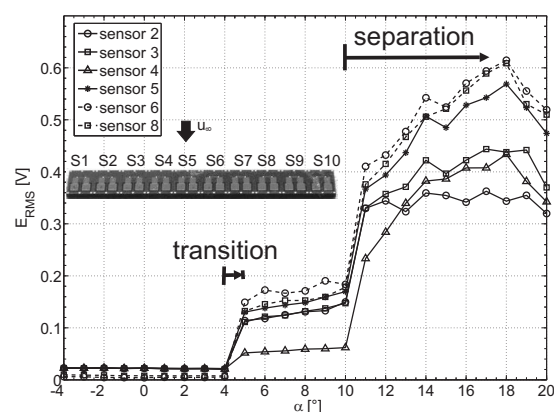


Fig. 7 RMS-values, MEMS-sensors,  $M_\infty = 0.2$

A further increase in the angle of attack causes a step-up of the adverse pressure gradient, leading to a pressure-induced turbulent trailing-edge separation. The separation induces massively increased RMS-levels for  $\alpha \geq 11^\circ$  (Fig. 7). The corresponding occurrence of laminar and turbulent flow as well as flow separation at all span-wise staggered sensors demonstrates the basically 2D character of the flow.

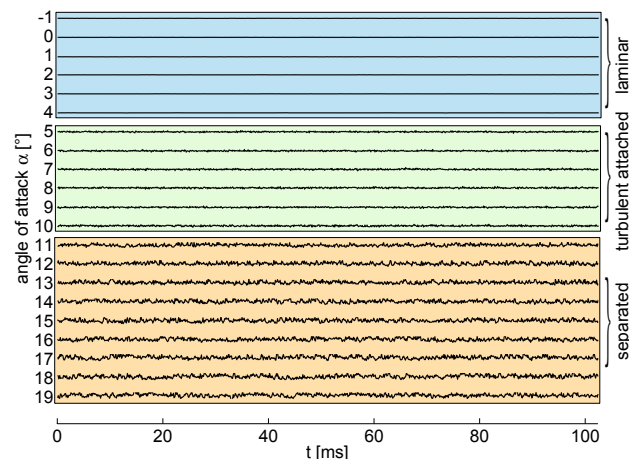
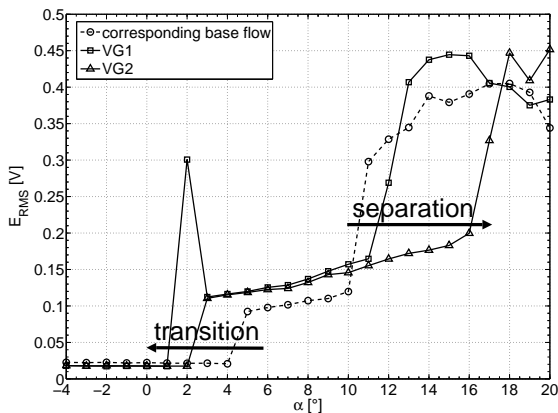


Fig. 8 Time-traces of one representative MEMS-sensor,  $M_\infty = 0.2$

In addition, Fig. 8 shows time-traces (*AC-values*) of one representative MEMS hot-film sensor (angles of attack increases from top to bottom). In accordance to the RMS, low AC-levels show the presence of attached laminar flow for  $\alpha \leq 4^\circ$ . In downward direction, an increasing angle of attack causes the boundary layer transition in the range  $4^\circ < \alpha < 5^\circ$  and leads to a fully turbulent flow up to angles of attack of  $\alpha \leq 10^\circ$  characterised by increased fluctuation amplitudes. Moreover, a significant rise in the dynamic signal amplitudes is detected for angles of attack of  $\alpha \geq 11^\circ$  since the flow separates due to the adverse pressure gradient.

#### 4.2 Passive actuation

Two kinds of vortex generators (Fig. 6) were applied at the leading edge of the slat to delay the flow separation. The influence of the passive devices on both transition and flow separation in comparison with the corresponding base flow is shown in Fig. 9. The RMS-levels clearly identify the forced laminar-turbulent transition induced by the passive devices. Additionally, such devices also intensify the momentum transfer and can decrease flow separation at the trailing edge of the slat.



**Fig. 9** Passive devices in comparison with the base flow, RMS-values of one representative MEMS-sensor,  $M_\infty = 0.2$

For the flow conditions illustrated ( $M_\infty = 0.2$ ), flow separation is suppressed

with the aid of VG1 and VG2 devices and higher angles of attack are reached. The RMS values clearly indicate the turbulent attached flow at  $3^\circ \leq \alpha \leq 11^\circ$  for VG1, whereas the VG2 nose can delay the separation up to  $\alpha > 16^\circ$ . Consequently, a further delay of flow separation is achieved with the larger vortex generator (VG2) because the shape of this passive device induces increased mixing.

The delay of flow separation using the passive devices was validated by the distribution of the pressure coefficients  $\hat{c}_{p_{max}}$  on the suction side as illustrated in Fig. 10. The maximum normalized pressure coefficient, which indicates a pre-separation state of the boundary layer, is shifted to  $\alpha = 12^\circ$  with a corresponding delta in maximum of  $\Delta \hat{c}_{p_{max}} \approx 0.12$  for VG1. Moreover, the maximum angle of attack is increased to  $\alpha_{max} = 14^\circ$  in comparison with the base flow for the VG2 vortex generator with an advantage of the maximum pressure coefficient  $\Delta \hat{c}_{p_{max}} \approx 0.21$ .

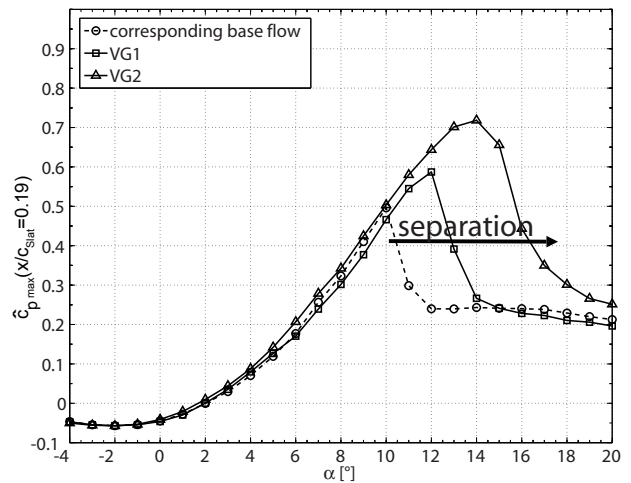


**Fig. 10**  $\hat{c}_{p_{max}}$ : corresponding base flow, VG1, VG2,  $M_\infty = 0.2$

Results of the flow affected by VG2 obtained with the high spatial resolution surface hot-wire array at the lower segment for the same free stream velocity ( $M_\infty = 0.2$ ) are presented in Fig. 11. Since each insert had a segment it was manufactured for, slight modifications of the slat contour were visible when changing the inserts between the two segments resulting in differing flow characteristics. Consequently, the turbu-

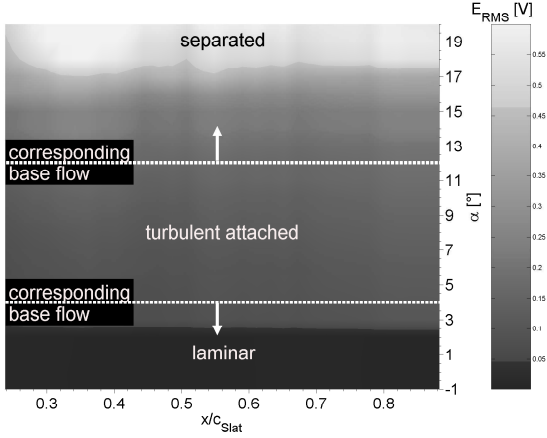


**Fig. 11** RMS-values of surface hot-wire array, VG2,  $M_\infty = 0.2$

lent attached flow without passive actuation is characterised by the dotted line in the range of  $4^\circ \leq \alpha \leq 12^\circ$ . It is shown, that the boundary layer transition is forced to  $2^\circ < \alpha < 3^\circ$  due to the influence of the VG2. Just like the corresponding base flow, the transition propagates upstream along the sensor array for  $x/c_{Slat} = 0.88$  up to  $x/c_{Slat} = 0.24$  at a variation of the angle of attack of  $\Delta\alpha = 1^\circ$ . Moreover, the positive influence of the forcing momentum induced by VG2 on flow separation is again clearly visible.

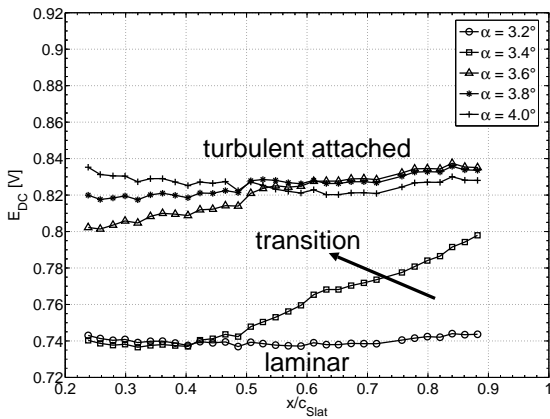


**Fig. 12** Mean values of surface hot-wire array,  $\Delta\alpha = 0.2^\circ$ ,  $M_\infty = 0.2$

Since the transition occurs very rapidly along the surface hot-wire array for  $\Delta\alpha = 1^\circ$ , mean values of the sensor signals for selected angles of attack with a variation of  $\Delta\alpha = 0.2^\circ$  are illustrated

in Fig. 12. The low mean values for  $\alpha = 3.2^\circ$  representing low shear stress levels are evidence for the presence of laminar flow. An increase in the angle of attack leads to a rise of the mean values at the trailing edge region that drops upstream. As the wall shear stress level in the turbulent flow is significantly higher than in the laminar one, this behaviour characterises the beginning of the boundary layer transition from the trailing edge. The transition propagates upstream for a further increase of the angle of attack and results in a fully turbulent flow for  $\alpha \geq 3.8^\circ$  along the sensor region.

### 4.3 Active actuation

A common feature of separated flows is the development of large scale vortex structures in conjunction with the typical vortex shedding. This highly dynamic process causes a mixture of fluid and a momentum transfer between the free flow and the recirculation area. For the investigation in hand, a fast magnetic valve was connected to a pressurised air supply system to generate a pulsed air flow at the leading edge of the slat (Fig. 1). This pulsed actuation at a chosen frequency of  $f = 110 \text{ Hz}$  ( $St_{c_{Slat}} = 0.2 - 0.39$ ) reduces the necessary perturbation momentum.

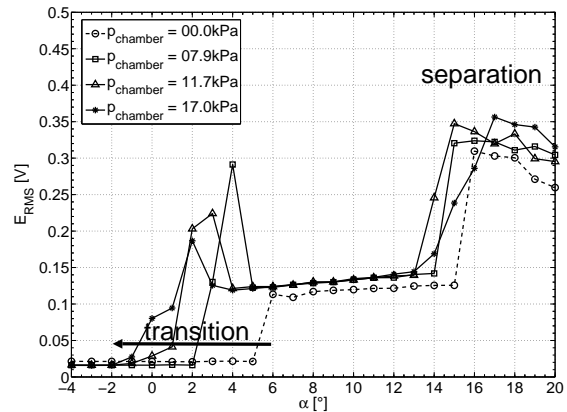


**Fig. 13** RMS-values of one representative MEMS-sensor: corresponding base flow vs. different mass flows at pulsed actuation,  $M_\infty = 0.1$

The RMS values for a single representative MEMS hot-film sensor at different actua-

tor chamber pressures and a free stream Mach number of  $M_\infty = 0.1$  are presented in Fig. 13. The transition is forced to lower angles of attack with increasing chamber pressures due to the increased momentum transfer. The rise of the RMS-values is also shifted to lower angles of attack indicating an accelerated onset of flow separation. However, the gradient of the RMS-distribution in the separation region is significantly reduced at an increased excitation rate compared to the corresponding base flow. The resulting improvement of the post-stall behaviour, characterised by the smooth rise of the RMS-level, is clearly confirmed by the distribution of the normalised maximum pressure coefficients  $\hat{c}_{p_{max}}$  in Fig. 14.

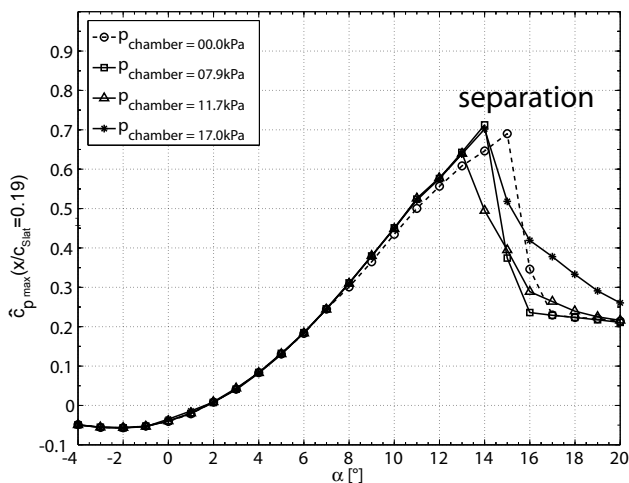


**Fig. 14**  $\hat{c}_{p_{max}}$ : corresponding base flow vs. different chamber pressures at pulsed actuation,  $M_\infty = 0.1$

For the presented chamber pressures the maximum angles of attack are lower than the reference pressure coefficient distribution for the corresponding base flow. However, the decrease in the pressure coefficients at higher angles of attack for pulsed actuation at different chamber pressures ( $p_{chamber} = 11.7 - 17.0$  kPa) is significantly smoother when compared to the corresponding base flow and validates the benefit in post-stall behaviour.

## 5 Summary

Measurements of an instrumented high-lift slat configuration at two different Mach numbers were performed using a stream-wise surface hot-wire array as well as a span-wise MEMS hot-film sensor array. As the boundary layer close to the leading edge of the slat was very thin, a cavity was machined into the slat to allow the sensor arrays to be flush-mounted so that disturbance to the flow by surface irregularities was minimised.

The results show that there is flow separation at high angles of attack on the high-lift device investigated. Additionally, laminar-turbulent transition takes place in the upstream section of the slat close to the leading edge for moderate angles of attack. The applied surface hot-wire technique is clearly capable of measuring the above-mentioned physical effects. Moreover, the newly designed MEMS hot-film sensors are also able to characterise these physical properties.

Both passive and active devices were used to control the separated flow. The two types of passive vortex generators investigated were shown to delay flow separation, with the VG2 type having a significantly greater effect than that obtained using the VG1. Furthermore, active devices were installed in the nose area in order to affect the flow by pulsed actuation. It was shown that whilst the devices did not delay separation, the post-stall behaviour was improved. In addition, the newly developed MEMS device proved to be a reliable and appropriate sensor for transition and separation detection. Even when placed in a single stream-wise position they reliably monitored both the laminar and turbulent boundary layer as well as the trailing edge separation.

## References

- [1] E. Greff. In-flight measurement of static pressures and boundary-layer state with integrated sensors. *Journal of Aircraft*, 28(5):289–299, 1991.
- [2] Y.S. Kachanov. Physical mechanisms of laminar-boundary-layer transition. *Annual Review of Fluid Mechanics*, 26:411–482, 1994.

- [3] H.-P. Kreplin and H. Denecke. Test report on surface hot film results, HPK050308-1, DLR, Göttingen. Technical report, AEROMEMS II Growth Project GRD1-2001-40167, Contract No G4RD-CT-2002-00748,, 2005.
- [4] I. Lee and H.J. Sung. Characteristics of wall pressure fluctuations in separated and reattaching flows over a backward-facing step: Part 1. *Experiments in Fluids*, 30:262–272, 2001.
- [5] J.C. Lin, S.K. Robinson, and R.J. McGhee. Separation control on high-lift airfoils via micro-vortex generators. *Journal of Aircraft*, 31(6):1317–1323, 1994.
- [6] R. Petz and W. Nitsche. Active separation control on a high-lift configuration by a periodically pulsating jet. In *Proceedings of the 24th ICAS Congress, Yokohama, Japan, 2004*.
- [7] A. Seifert, A. Darabi, and I. Wygnanski. Delay of airfoil stall by periodic excitation. *Journal of Aircraft*, 33(4):691–698, 1996.
- [8] D. Sturzebecher, S. Anders, and W. Nitsche. The surface hot-wire as a means of measuring mean and fluctuating wall-shear stresses. *Experiments in Fluids*, 31:294–301, 2001.
- [9] F. Tinapp and W. Nitsche. Separation control on a high-lift configuration by periodic excitation. In S. Wagner, U. Rist, H.J. Heinemann, and R. Hilbig, editors, *Notes on Numerical Fluid Dynamics*, volume 77 of *New Results in Numerical and Experimental Fluid Mechanics III*, pages 181–188. Springer-Verlag, 2001.